High Resolution Pulsed Field Ionization−Photoelectron Bands for $CS_2^+(\tilde{A}^2\Pi_u)$: An Experimental and Theoretical Study†

Jianbo Liu

Chemical Sciences Division, Lawrence Berkeley National Laboratory, Berkeley, California 94720

M. Hochlaf, G. Chambaud, and P. Rosmus

Theoretical Chemistry Group, University of Marne-La−Vallée, Champs sur Marne, F-77454, Marne-la-Vallée, France

C. Y. Ng*

Ames Laboratory, USDOE, and Department of Chemistry, Iowa State University, Ames, Iowa 50011

Received: May 31, 2000; In Final Form: July 31, 2000

The vacuum ultraviolet pulsed field ionization−photoelectron (PFI−PE) spectra for CS_2 were measured in the full energy range of 12.6−13.5 eV, revealing complex vibronic band structures for the $CS_2^+(\tilde{A}^2\Pi_u)$ state. Three-dimensional potential energy functions (PEFs) for $CS_2^+(\tilde{A}^2\Pi_u)$ were also generated theoretically using the complete active space self-consistent field and internally contracted multireference configuration interaction methods. Using these PEFs, the harmonic frequencies, anharmonic constants, and Renner−Teller rovibronic energy levels for $CS_2^+(\tilde{A}^2\Pi_u)$ were calculated variationally. Many Fermi polyads have been identified in the rovibronic states of $CS_2^+(\tilde{A}^2\Pi_u)$. Using present theoretical and available optical data, we assigned most of the PFI−PE rovibronic bands due to excitation of the ν_1^+ (symmetric stretching), ν_2^+ (bending), and ν_3^+ (asymmetric stretching) modes for $CS_2^+(\tilde{A}^2\Pi_u)$. The simulation of rotational contours resolved in the high-resolution PFI−PE bands for $CS_2^+(\tilde{A}^2\Pi_u)$; $\nu_1^+ = 0-3$, $\nu_2^+ = 0,2$, $\nu_3^+ = 0$) provided accurate ionization energies for the formation of these states from $CS_2(\tilde{X}^1\Sigma_g^+)$.

I. Introduction

Being a molecule of astrophysical and aeronomic interest,[1] the spectroscopy of the CS_2 and its cation CS_2^+ has been examined extensively by numerous experimental techniques. These include studies using emission spectroscopy,[2−4] laser-induced fluorescence,[5,6] absorption,[6−8] vacuum ultraviolet (VUV) photoionization mass spectrometry,[9−12] photoelectron spectroscopy [including HeI,[13−21] HeII,[21] threshold photoelectron (TPE)[22] and pulsed field ionization−photoelectron (PFI−PE) spectroscopy[11,12]], and photoelectron−photon coincidence spectroscopy.[23] When combined with state-of-the-art theoretical investigations,[24−27] the previous experimental studies yielded valuable information about the vibronic structures of CS_2^+. The previous HeI,[13−21] HeII,[21] and TPE[22] studies of CS_2 provided unambiguous identification of some vibronic bands for the first four valence ionic states $CS_2^+(\tilde{X}^2\Pi_g, \tilde{A}^2\Pi_u, \tilde{B}^2\Sigma_u^+$ and $\tilde{C}^2\Sigma_g^+)$. Furthermore, these studies revealed many spectroscopic features that are of theoretical interest, such as those arising from spin−orbit interactions, Renner−Teller coupling, and anharmonic resonances. The observation of symmetry-forbidden excitation involving one quantum of the bending vibration ν_2^+ and the breakdown of the molecular orbital scheme in photoionization transition, in particular, are noted.

The HeI photoelectron bands obtained for $CS_2^+(\tilde{X}^2\Pi_g$ and $\tilde{A}^2\Pi_u)$ clearly revealed strong interactions due to Fermi resonances between levels involving the symmetric stretching vibration ν_1^+ and overtones of the bending vibration ν_2^+. However, partly due to the relatively low resolution used, none of the previous HeI photoelectron measurements were able to completely resolve rovibronic structures associated with these vibronic states. As a result, many discrepancies in the spectral interpretation have occurred. The recent PFI−PE measurements on the study of $CS_2^+(\tilde{X}^2\Pi_g)$ using nonresonant two-photon (N2P)[11] and VUV laser source[12] have significantly improved the photoelectron resolution to a few cm^{-1}. These high-resolution laser-based PFI−PE studies, together with ab initio theoretical calculations, have made possible the identification of most of the rovibronic structures, resulting in the determination of more accurate ionization energies (IEs) for these states. However, because of the difficulty in generating a wide tunable photon energy range using the N2P and VUV laser sources, the high-resolution PFI−PE studies have been limited to the first $CS_2^+(\tilde{X}^2\Pi_g)$ electronic band.[11,12]

Recently, a high-resolution VUV monochromatized undulator synchrotron source in the photon energy range of 6−30 eV has been established at the Chemical Dynamics Beamline of the Advanced Light Source (ALS) associated with the Lawrence Berkeley National Laboratory.[28−30] Taking advantage of this high-resolution VUV facility, we developed novel synchrotron-based PFI−PE detection schemes,[31−33] achieving resolution similar to that attained in laser-based studies. The most attractive feature of the synchrotron light is its ease of tunability, making high-resolution PFI−PE measurements for many molecules in a large energy region a routine operation.[34−41] Using the high-

† Part of the special issue "Aron Kuppermann Festschrift".

* To whom correspondence should be addressed (E-mail: CYNG@AMESLAB.GOV).

10.1021/jp001998n CCC: $20.00
Published on Web 10/13/2000

resolution synchrotron-based PFI−PE technique, we obtained the PFI−PE spectrum of CS_2 in the full energy range of 12.6−17.2 eV, covering the formation of $CS_2^+(\tilde{A}^2\Pi_u, \tilde{B}^2\Sigma_u^+$, and $C^2\Sigma_g^+)$ states and the satellite states[21] for CS_2^+ appearing in this region. As expected, this PFI−PE measurement reveals many new rovibronic features, which were not resolved or accessible to HeI photoelectron spectroscopic[13−21] measurements.

To provide a reliable interpretation of the PFI−PE data, we also performed a high level ab initio study of CS_2^+. We generated theoretically the three-dimensional potential energy functions (PEFs) for CS_2^+. On the basis of these PEFs, we have calculated the rovibronic energy levels for the CS_2^+ ionic states using a Renner−Teller variational approach. With the aid of such theoretical predictions, we are able to make unambiguous identification of individual rovibronic bands for $CS_2^+(\tilde{A}^2\Pi_u)$. On the basis of spectral simulations of the high-resolution PFI−PE bands, we obtained accurate values for IE with uncertainties ≤ 4 cm^{-1}. This article describes the analysis of PFI−PE data for ionization transitions $CS_2^+(\tilde{A}^2\Pi_u; \nu_1^+ = 0-6, \nu_2^+ = 0-4, \nu_3^+ = 0-1) \leftarrow CS_2(\tilde{X}^1\Sigma_g^+; \nu_1'' = 0-1, \nu_2'' = 0-1, \nu_3'' = 0)$, where ν_1^+ (ν_1''), ν_2^+ (ν_2''), and ν_3^+ (ν_3'') represent the symmetric stretching mode, the bending mode and the asymmetric stretching mode, respectively, for $CS_2^+(\tilde{A}^2\Pi_u)$ [$CS_2(\tilde{X}^1\Sigma_g^+)$]. The analysis of PFI−PE spectra for the $CS_2^+(\tilde{B}^2\Sigma_u^+$ and $\tilde{C}^2\Sigma_g^+)$ states will be reported in a separate paper.

II. Experimental Methods and Theoretical Calculations

A. Experimental Methods. The experiment was carried out at the Chemical Dynamics Beamline of the ALS. The beamline consisted of a 10 cm period undulator, a gas harmonic filter, a 6.65 m off-plane Eagle mounted monochromator, and a multipurpose photoelectron−photoion apparatus, all of which were described in previous publications.[28−33]

In the present experiment, helium was used in the harmonic gas filter to suppress the higher undulator harmonics with photon energies greater than 24.59 eV. Undulator light of the first harmonic emerging from the gas filter was directed into the monochromator and dispersed by a 4800 lines/mm grating (dispersion = 0.32 Å/mm) before entering the photoelectron−photoion apparatus. The monochromator entrance/exit slits used were in the range of 30/30−300/300 μm, corresponding to nominal wavelength resolutions in the range of 0.009−0.095 Å (full width at half-maximum (fwhm)).

The CS_2 sample was introduced into the photoionization/photoexcitation (PI/PEX) region in the form of a neat CS_2 beam formed by supersonic expansion through a stainless steel nozzle (nozzle diameter = 0.127 mm) at a stagnation pressure of about 300 Torr. The supersonic beam was produced using a two-stage differentially pumped arrangement. The CS_2 beam was skimmed by a circular skimmer (diameter = 1 mm) prior to entering the PI/PEX region of the photoelectron−photoion apparatus. The first and second differentially pumping chambers were evacuated by turbomolecular pumps with pumping speeds of 2000 and 1200 L/s, and maintained pressures of 6×10^{-4} and 9×10^{-6} Torr, respectively, during the experiment.

The procedure for multibunch synchrotron-based PFI−PE measurements was described in detail previously.[31] In this experiment, the ALS storage ring was filled with 328 electron buckets in a period of 656 ns. Each electron bucket emits a light pulse of 50 ps with a time separation of 2 ns between successive buckets. In each storage ring period, there is a 16 ns dark gap consisting of eight consecutive unfilled buckets for the ejection of cations from the ring orbital. A nominally zero electrostatic dc field was maintained across the PI/PEX region prior to the application of a pulsed electric field to the repeller plates on both sides of the PI/PEX region. The pulsed field used was 0.54 V/cm in height and 42 ns in width, which centered at the 16 ns dark gap. In the present study, the pulsed electrical field for pulsed field ionization was applied every other synchrotron ring period, i.e., 1.312 μs, corresponding to a repetition rate of 0.76 MHz.

The intensity for the monochromatized VUV beam was monitored by a tungsten photoelectric detector. The VUV detection efficiency as a function of the VUV photon energy for this tungsten detector was corrected using the known photoelectric yield curve.[42] Spectra presented here were flux normalized by the corresponding VUV photon intensities. The energy step sizes used were in the range of 0.15−0.5 meV and the counting times for each step varied in the range of 4−8 s.

All PFI−PE spectra were calibrated before and after each experimental run using either the $Xe^+(^2P_{3/2})$ and $Kr^+(^2P_{3/2})$ PFI−PE bands, or the $Ar^+(^2P_{3/2})$ and $Kr^+(^2P_{3/2})$ PFI−PE bands, obtained under the same experimental conditions.[30,43] The calibration scheme assumes that the Stark shifts for the IEs of CS_2 and the rare gases are identical. Previous measurements indicate that the accuracy of this calibration method is within ±0.5 meV.[35]

B. Theoretical Calculations for the $CS_2^+(\tilde{A}^2\Pi_u)$ State. The PEFs of the $CS_2^+(\tilde{A}^2\Pi_u)$ state were calculated using the complete active space self-consistent field (CASSCF)[44] and internally contracted multireference configuration interaction (MRCI) methods.[45,46] In these calculations, the generally contracted spdf cc-VQZ basis set of Dunning was used.[47] All valence molecular orbitals were active. In the CASSCF calculations, the Hartree−Fock molecular orbitals for the neutral $CS_2(\tilde{X}^1\Sigma_g^+)$ were used because of the symmetry-breaking problem in the restricted Hartree−Fock wave functions. In all calculations, the $CS_2^+(\tilde{X}^2\Pi_g$ and $\tilde{A}^2\Pi_u)$ states were averaged and optimized together with equal weights. For MRCI calculations, all configurations with coefficients larger than 0.01 in the CI expansions of the CASSCF wave functions were used as a reference in the subsequent MRCI calculations. The electronic calculations were carried out using the MOLPRO program suite.[48]

The calculations were performed for 22 different geometries covering the region of ≈10000 cm^{-1} above the equilibrium minimum of the $CS_2^+(\tilde{A}^2\Pi_u)$ electronic state and geometry ranges $2.6 < R_{CS} < 3.6$ bohr and $140° < \theta < 180°$, where R_{CS} is the C−S distance and θ is the S−C−S angle. The MRCI energies were fitted to polynomial expansions in displacement coordinates for both Renner−Teller components. These PEFs expansions were used to calculate the quartic force fields in internal coordinates, which were transformed by the *l*-tensor algebra to the quartic force fields in dimensionless normal coordinates. The resulting force fields and some spectroscopic constants for the $CS_2^+(\tilde{A}^2\Pi_u)$ states are listed in Table 1. The values for the upper component are given in parentheses.

The Renner−Teller problem was solved variationally for J up to 9/2. In these calculations, the full dimensionality, anharmonicity, rotation−vibration, electronic angular momenta, and spin−orbit coupling effects are considered. In the Hamiltonian the $A_{so}\cdot\boldsymbol{L}\cdot\boldsymbol{S}$ term was replaced by $A_{so}\cdot L_z S_z$. For the A_{so} spin−orbit constant, the experimental value of −177.4 cm^{-1} was used. Details of the variational calculations can be found in refs 49 and 50.

C. Simulation of Rotational Transition Intensities. The relative intensities for rotational structures observed in the high-

TABLE 1: Calculated Spectroscopic Constants (R_e, ϵ A_{so}, and B^+), Harmonic Frequencies (ω_1, ω_2, and ω_3), and Quartic Force Field (Φ) of $CS_2^+(\tilde{A}^2\Pi_u)$ in Dimensionless Normal Coordinates

parameters [a]	$\tilde{A}^2\Pi_u$
R_e	1.624
ϵ	0.251
A_{so} [b]	−173.56
B^+	0.0999
ω_1	576.8
ω_2	261.8 (328.4) [c]
ω_3	1753.6
Φ_{111}	−107.4
Φ_{122}	122.8 (94.3) [c]
Φ_{133}	−198.5
Φ_{1111}	16.7
Φ_{2222}	69.6 (54.6) [c]
Φ_{3333}	−214.7
Φ_{1122}	−26.4 (−17.1) [c]
Φ_{2233}	−67.2 (−10.1) [c]
Φ_{1133}	37.7

[a] R_e are in Å, ϵ is Renner−Teller parameter for (0,1,0) $A^2\Pi_u$. All other parameters are in cm^{-1}. [b] Calculated from CASSCF wavefunctions. [c] Values in parentheses refer to the other Renner−Teller component.

resolution PFI−PE bands were simulated using the Buckingham−Orr−Sichel (BOS) model.[51] This model was derived to predict relative transition line strengths observed in single-photon ionization of diatomic molecules and can be extended to linear triatomic molecules.[53] The rotational line strengths are given by eq 1,

$$\sigma_{J^+\leftarrow J''} \propto \sum_{\lambda} C_\lambda Q(\lambda, J'', J^+) \quad (1)$$

where J'' and J^+ are the total angular momenta for the neutral and ionic states, respectively. The BOS coefficient C_λ is associated with the electronic transition moments, which are the linear combination of electron transition amplitudes for the possible orbital angular momentum l of the ejected electron. The parameter λ can be considered as the orbital angular momentum of the electron prior to photoexcitation and is restricted by

$$l - 1 \le \lambda \le l + 1 \quad (2)$$

The other factor $Q(\lambda, J'', J^+)$ represents the Clebsch−Gordan coefficients for the Hund's coupling case (a).[52] The BOS simulations of the PFI−PE bands are purely empirical in nature, aiming mainly to deduce more accurate IE values for these bands.

The simulation used rotational constant $B'' = 0.1091$ cm^{-1} for the neutral ground state[52] and rotational constant B^+ for the ionic state taken from ref 3. A Gaussian instrumental line shape with a fwhm of 3−6 cm^{-1} was used to simulate the observed rotational contours. We find that a rotational temperature of 60−100 K for CS_2 yields the best fits for the experimental PFI−PE bands.

III. Results and Discussion

The ground state of neutral CS_2 ($\tilde{X}^1\Sigma_g^+$) is linear with the dominating electronic configuration[24] $(core)^{22}(5\sigma_g)^2(4\sigma_u)^2(6\sigma_g)^2(5\sigma_u)^2(2\pi_u)^4(2\pi_g)$.[4] The first excited vibrational levels for ν_1'', ν_2'', and ν_3'' of $CS_2(\tilde{X}^1\Sigma_g^+)$ are known to be at 658, 396, and 1535 cm^{-1}, respectively.[52] Removing an electron from the $2\pi_g$, $2\pi_u$, $5\sigma_u$, and $6\sigma_g$ orbitals results in the $CS_2^+(\tilde{X}^2\Pi_g, \tilde{A}^2\Pi_u, \tilde{B}^2\Sigma_u^+$, and $\tilde{C}^2\Sigma_g^+)$ states, respectively. The PFI−PE spectrum in the energy region of 12.6−17.2 eV, covering the region for the formation of the $CS_2^+(\tilde{A}^2\Pi_u)$, $\tilde{B}^2\Sigma_u^+$, and $\tilde{C}^2\Sigma_g^+$) states, as well as some shake-up states of CS_2^+, is shown in Figure 1. The present work deals only with the first electronically excited $CS_2^+(\tilde{A}^2\Pi_u)$ state. The C−S equilibrium distance (R_e) for $CS_2^+(\tilde{A}^2\Pi_u)$ is calculated to be 1.624 Å (Table 1), distinctly longer than in the neutral molecule (1.554 Å).[52] This calculation predicts that many vibronic states for $CS_2^+(\tilde{A}^2\Pi_u)$ are formed upon VUV photoionization of CS_2.

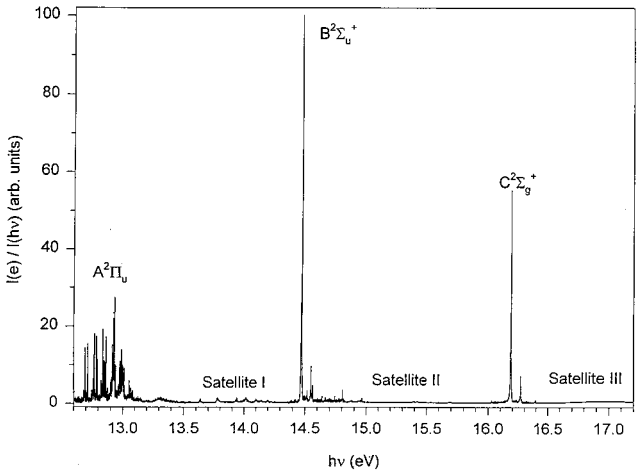

Figure 1. PFI−PE spectrum for the $CS_2^+(\tilde{A}^2\Pi_u, \tilde{B}^2\Sigma_u^+$, and $\tilde{C}^2\Sigma_g^+)$ states as well as three satellite states associated with $\tilde{A}^2\Pi_u$ in the region of 12.6−17.2 eV obtained at a PFI−PE resolution of 7 cm^{-1} (fwhm).

A. Theoretical Vibronic Levels for $CS_2^+(\tilde{A}^2\Pi_u)$. The vibronic levels of an electronically degenerate open shell state of a triatomic molecule can be classified according to $K = \Lambda + l_i$ and $P = \Lambda + l_i + \Sigma$, the projections of the angular momenta along the linear axis. For a $^2\Pi$ state, $\Lambda = \pm 1$, $\Sigma = \pm 1/2$, and l_i can take values ν_i, $\nu_i - 2$, $\cdots$, $-\nu_i$. The calculated vibronic levels for $CS_2^+(\tilde{A}^2\Pi_u)$ are listed in Table 2. The symmetry symbols Σ, Π, Δ, Φ, and Γ in Table 2 correspond to $K = 0$, 1, 2, 3, and 4, respectively. The upper index relates to an electronic doublet state, while the lower index corresponds to the P value. For $K > 0$, the pattern begins with "unique levels", which split only in P. For higher quanta in ν_2, the vibronic bending levels split into μ and κ levels (lower and upper components, respectively) due to the Renner−Teller coupling.

In the vibrational progressions of linear−linear transitions, only the totally symmetric stretching ν_1^+, the even quanta of the bending $2\nu_2^+$, and even quanta of the asymmetric stretching $2\nu_3^+$ progressions are allowed. The last two modes are usually weak. However, as in the electronic ground state of CS_2^+ (ref 12), the $CS_2^+(\tilde{A}^2\Pi_u)$ state exhibits strong Fermi resonance interactions between ν_1^+ and $2\nu_2^+$, which lead to intensity changes in the rovibronic progressions. In Figure 2, we depict the vibrational part of the wave functions of the levels $(1,0,0)^2\Pi_{1/2}$ and $(0,2,0)\kappa^2\Pi_{1/2}$ forming such an anharmonic resonance. For energies higher than 1700 cm^{-1} [relative to the $(0,0,0)^2\Pi_{3/2}$ level] the anharmonic effects are so strong that an unambiguous assignment with harmonic quantum numbers becomes hardly possible. For example, the $^2\Pi_{3/2}$ level at 1930.3 cm^{-1} (see Table 2) is a mixture of the $(2,2,0)\kappa^2\Pi_{3/2}$, $(0,6,0)\kappa^2\Pi_{3/2}$, and $(1,4,0)\kappa^2\Pi_{3/2}$ components of the Fermi polyad $2\nu_1^+ + \nu_2^+ = 6$, and the $(1,6,0)\mu^2\Pi_{3/2}$ and $(0,8,0)\mu^2\Pi_{3/2}$ components of the Fermi polyad $2\nu_1^+ + \nu_2^+ = 8$. The Fermi resonances of $CS_2^+(\tilde{A}^2\Pi_u)$ have been discussed for a long time, however, they have never been clearly identified in the HeI spectra. Bondybey et

TABLE 2: Calculated Vibronic Levels for $CS_2^+(\tilde{A}^2\Pi_u)$

state	calc. (cm^{-1})[a]	state	calc. (cm^{-1})
$^2\Sigma^+$ levels		$^2\Sigma^-$ levels	
$(0,1,0)_\mu$	271.3	$(0,1,0)_\kappa$	500.0
$(0,3,0)_\mu/(1,1,0)_\mu$	767.7	$(1,1,0)_\kappa/(0,3,0)_\kappa$	1051.2
$(1,1,0)_\mu/(0,3,0)_\mu$	886.5	$(0,3,0)_\kappa/(1,1,0)_\kappa$	1174.9
$(0,5,0)_\mu/(1,3,0)_\mu$	1244.9	$(2,1,0)_\kappa/(1,3,0)_\kappa/(0,5,0)_\kappa$	1597.9
$(2,1,0)_\mu/(1,3,0)_\mu/(0,5,0)_\mu$	1387.0	$(0,5,0)_\kappa/(2,1,0)_\kappa/(1,5,0)_\mu/(0,7,0)_\mu$	1685.9
$(2,1,0)_\mu/(1,3,0)_\mu$	1509.8	$(0,5,0)_\kappa/(1,3,0)_\kappa/(2,3,0)_\mu$	1855.4
$(0,7,0)_\mu/(2,1,0)_\kappa/(1,3,0)_\kappa$	1736.7	$(2,3,0)_\kappa/(3,1,0)_\kappa$	2163.5
$(0,7,0)_\mu/(1,3,0)_\kappa/(2,3,0)_\kappa$	1896.4	$(0,1,1)_\kappa$	2218.3
$(0,1,1)_\mu$	1974.4	$(3,1,0)_\kappa/(0,7,0)_\kappa/(1,5,0)_\kappa$	2274.2
$(3,1,0)_\mu/(1,5,0)_\mu$	2009.4	$(0,7,0)_\kappa/(2,3,0)_\kappa/(3,1,0)_\kappa$	2427.0
$(0,9,0)_\mu/(1,5,0)_\kappa$	2115.0		
$(2,3,0)_\mu/(1,5,0)_\mu/(3,1,0)_\mu$	2143.0		
$(0,9,0)_\mu/(2,5,0)_\mu/(3,3,0)_\mu$	2327.7		
$(0,3,1)_\mu$	2462.3		
$^2\Pi_{1/2}$ levels		$^2\Pi_{3/2}$ levels	
(0,0,0)	174.1	(0,0,0)	0
$(0,2,0)_\mu$	548.6	$(0,2,0)_\mu/(1,0,0)$	518.6
$(1,0,0)/(0,2,0)_\kappa$	737.0	$(1,0,0)/(0,2,0)_\mu$	598.2
$(0,2,0)_\kappa/(1,0,0)$	825.2	$(0,2,0)_\kappa$	824.6
$(0,4,0)_\mu/(1,2,0)_\mu$	1026.8	$(0,4,0)_\mu/(1,2,0)_\mu$	1005.1
$(1,2,0)_\mu/(0,4,0)_\mu$	1176.5	$(2,0,0)/(0,4,0)_\mu/(1,2,0)_\mu$	1122.8
$(2,0,0)/(1,2,0)_\kappa$	1295.0	$(1,2,0)_\mu/(2,0,0)$	1207.7
$(2,0,0)/(0,4,0)_\kappa/(1,2,0)_\kappa$	1376.1	$(1,2,0)_\kappa/(0,4,0)_\kappa$	1367.4
$(0,6,0)_\mu/(1,4,0)_\mu$	1481.0	$(0,6,0)_\kappa/(1,4,0)_\mu$	1468.1
$(0,4,0)_\kappa/(1,2,0)_\kappa/(0,6,0)_\mu$	1523.6	$(0,4,0)_\kappa/(1,2,0)_\kappa$	1525.0
$(2,2,0)_\mu/(0,6,0)_\mu/(1,4,0)_\mu$	1659.6	$(2,2,0)_\mu/(0,6,0)_\mu/(1,4,0)_\mu/(3,0,0)$	1626.0
$(2,2,0)_\mu/(1,4,0)_\mu$	1811.3	(0,0,1)	1709.7
$(2,2,0)_\kappa/(3,0,0)/(1,4,0)_\kappa$	1845.0	$(3,0,0)/(1,4,0)_\mu$	1726.4
(0,0,1)	1882.8	$(2,2,0)_\mu/(1,4,0)_\mu/(3,0,0)$	1830.6
$(0,8,0)_\mu/(3,0,0)/(1,6,0)_\mu$	1906.2	$(0,8,0)_\mu/(1,4,0)_\kappa/(2,2,0)_\kappa$	1895.2
$(3,0,0)/(1,6,0)_\mu/(0,6,0)_\kappa$	1960.0	$(2,2,0)_\kappa/(1,6,0)_\mu/(0,8,0)_\mu/(0,6,0)_\kappa/(1,4,0)_\kappa$	1930.3
$(2,2,0)_\kappa/(0,6,0)_\kappa/(0,8,0)_\kappa$	2059.1	$(2,2,0)_\kappa/(0,6,0)_\kappa/(1,4,0)_\kappa$	2061.5
$(2,4,0)_\mu/(0,6,0)_\kappa/(0,8,0)_\mu$	2124.1	$(2,4,0)_\mu/(0,8,0)_\mu/(3,2,0)_\mu$	2102.7
$(1,4,0)_\kappa/(0,6,0)_\kappa/(0,8,0)_\mu$	2224.9	$(0,2,1)_\mu$	2219.6
$(0,2,1)_\mu$	2248.2	$(1,4,0)_\kappa/(3,2,0)_\mu/(3,0,0)$	2228.8
$(3,2,0)_\mu/(1,6,0)_\mu/(0,6,0)_\kappa$	2300.3	$(0,6,0)_\kappa/(1,4,0)_\kappa/(3,0,0)$	2253.3
$(0,10,0)_\mu/(1,8,0)_\mu$	2343.9	(1,0,1)	2305.4
$(3,2,0)_\kappa/(3,0,0)/(2,4,0)_\kappa$	2410.1	$(3,0,0)/(1,6,0)_\mu/(2,4,0)_\mu$	2336.0
(1,0,1)	2448.8	$(0,10,0)_\mu/(1,8,0)_\mu$	2347.1
$^2\Delta_{3/2}$ levels		$^2\Delta_{5/2}$ levels	
(0,1,0)	459.7	(0,1,0)	291.7
$(0,3,0)_\mu$	829.6	$(0,3,0)_\mu/(1,1,0)$	782.8
$(1,1,0)/(0,3,0)_\kappa$	1022.5	$(1,1,0)/(0,3,0)_\mu$	898.8
$(0,3,0)_\kappa/(1,1,0)$	1133.8	$(0,3,0)_\kappa$	1147.8
$(0,5,0)_\mu/(1,3,0)_\mu$	1293.7	$(0,5,0)_\mu/(1,3,0)_\mu$	1252.0
$(1,3,0)_\mu/(0,5,0)_\mu$	1467.9	$(2,1,0)/(1,3,0)_\mu/(0,5,0)_\mu$	1399.7
$(2,1,0)/(1,3,0)_\kappa/(0,5,0)_\kappa$	1577.9	$(2,1,0)/(1,3,0)_\mu$	1515.1
$(0,5,0)_\kappa/(2,1,0)/(1,3,0)_\kappa$	1672.7	$(1,3,0)_\kappa/(0,5,0)_\kappa$	1681.9
$(0,7,0)_\mu/(1,5,0)_\mu$	1752.8	$(0,7,0)_\mu/(1,5,0)_\mu$	1708.3
$(0,5,0)_\kappa/(1,3,0)_\kappa$	1835.9	$(0,5,0)_\kappa/(1,3,0)_\kappa$	1861.6
$(2,3,0)_\mu/(0,7,0)_\mu/(1,5,0)_\mu$	1941.2	$(2,3,0)_\mu/(0,7,0)_\mu$	1883.7
$(2,3,0)_\mu/(1,5,0)_\mu/(3,1,0)$	2104.1	(0,1,1)	2000.5
$(2,3,0)_\mu/(1,5,0)_\mu$	2120.5	$(3,1,0)/(1,5,0)_\mu$	2016.8
(0,1,1)	2165.4	$(0,9,0)_\mu/(1,7,0)_\mu/(2,3,0)_\mu$	2139.3
$(3,1,0)/(0,9,0)_\mu/(1,7,0)_\mu/(2,3,0)_\kappa$	2171.7	$(2,3,0)_\mu/(3,1,0)/(1,5,0)_\mu$	2144.0
$(3,1,0)/(0,7,0)_\kappa/(1,5,0)_\kappa$	2260.5	$(2,3,0)_\kappa/(1,5,0)_\kappa/(0,7,0)_\kappa$	2225.6
$(0,9,0)_\mu/(2,5,0)_\mu/(1,7,0)_\kappa$	2349.4	$(2,5,0)_\mu/(0,9,0)_\mu/(3,3,0)_\mu$	2341.6
$(0,7,0)_\kappa/(2,3,0)_\kappa$	2416.6	$(2,3,0)_\kappa/(0,7,0)_\kappa$	2398.9
		$(0,3,1)_\mu$	2480.0
$^2\Phi_{5/2}$ levels		$^2\Phi_{7/2}$ levels	
(0,2,0)	738.9	(0,2,0)	579.6
$(0,4,0)_\mu$	1111.4	$(0,4,0)_\mu/(1,2,0)$	1049.0
$(1,2,0)/(0,4,0)$	1307.7	$(1,2,0)/(0,4,0)_\mu$	1194.6
$(0,4,0)_\kappa/(1,2,0)$	1432.4	$(0,4,0)_\kappa$	1470.0
$(0,6,0)_\mu/(1,4,0)_\mu$	1565.6	$(0,6,0)_\mu/(1,4,0)_\mu$	1503.0
$(1,4,0)_\mu/(0,6,0)_\mu$	1758.2	$(2,2,0)/(1,4,0)_\mu/(0,6,0)_\mu$	1676.5
$(1,4,0)_\kappa/(2,2,0)$	1863.3	$(2,2,0)\ /(1,4,0)_\mu$	1817.6
$(0,8,0)_\mu/(2,2,0)$	1952.7	$(0,8,0)_\mu/(1,6,0)_\mu$	1943.8
$(0,10,0)_\mu/(1,6,0)_\mu/(1,4,0)_\kappa/(2,2,0)$	2036.0	$(1,4,0)_\kappa/(0,6,0)_\kappa$	2004.2
$(0,8,0)_\mu/(1,4,0)_\kappa/(1,6,0)_\mu$	2136.6	$(2,4,0)_\mu/(0,8,0)_\mu/(1,6,0)_\mu$	2140.8
$(0,10,0)_\mu/(2,4,0)_\mu/(1,6,0)_\mu$	2231.8	$(0,6,0)_\kappa/(1,4,0)_\kappa$	2201.0
$(0,12,0)_\mu/(1,8,0)_\mu/(2,4,0)_\kappa$	2366.6	(0,2,1)	2286.2
$(1,6,0)_\mu/(2,4,0)_\mu/(3,2,0)$	2411.9	$(3,2,0)/(1,6,0)_\mu$	2304.0
(0,2,1)	2440.1	$(0,10,0)_\mu/(1,8,0)_\mu$	2374.9

TABLE 2 (Continued)

state	calc. (cm^{-1})[a]	state	calc. (cm^{-1})
$^2\Gamma_{7/2}$ levels		$^2\Gamma_{9/2}$ levels	
(0,3,0)	1012.6	(0,3,0)	863.7
$(0,5,0)_\mu$	1390.9	$(0,5,0)_\mu/(1,3,0)$	1315.4
$(1,3,0)/(0,5,0)_\kappa$	1592.9	$(1,3,0)/(0,5,0)_\mu$	1486.7
$(0,5,0)_\kappa/(1,3,0)$	1723.8	$(0,7,0)_\mu/(1,5,0)_\mu$	1756.1
$(0,7,0)_\mu/(1,5,0)_\mu$	1840.7	$(0,5,0)_\kappa$	1791.4
$(1,5,0)_\mu/(0,7,0)_\mu$	2044.8	$(1,5,0)_\mu/(2,3,0)/(0,7,0)_\mu$	1952.4
$(1,5,0)_\kappa/(2,3,0)/(0,9,0)_\mu$	2148.7	$(2,3,0)/(1,5,0)_\mu$	2116.8
$(2,3,0)/(0,9,0)_\mu/(1,7,0)_\mu$	2227.4	$(0,9,0)_\mu/(1,7,0)_\mu$	2187.6
$(0,7,0)_\kappa/(1,5,0)_\kappa/(1,7,0)_\mu/(2,3,0)_\mu$	2326.3	$(1,3,0)/(0,5,0)_\kappa$	2321.0
$(0,9,0)_\mu/(1,5,0)_\kappa/(2,5,0)_\mu$	2425.1	$(2,5,0)_\mu/(0,9,0)_\mu/(1,7,0)_\mu$	2402.6

[a] The energies are given relative to the $(0,0,0)^2\Pi_{3/2u}$ state.

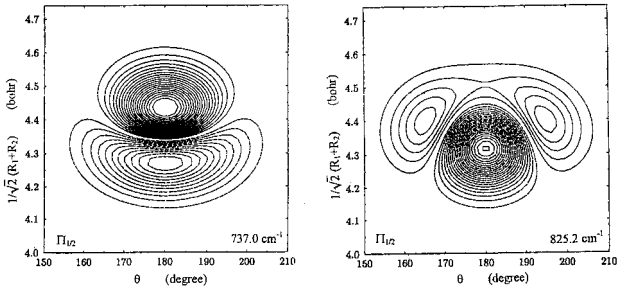

Figure 2. Fermi resonance between the $(1,0,0)^2\Pi_{1/2}$ and the $(0,2,0)\kappa^2\Pi_{1/2}$ rovibronic levels in the $CS_2^+(\tilde{A}^2\Pi_u)$ state (R_1 and R_2 are both CS distances and θ is the S−C−S angle).

al.[5,6] assigned ν_1^+ at 560 cm^{-1} and $2\nu_2^+$ at 621 cm^{-1}, based on the laser-induced $\tilde{X}^2\Pi_g \rightarrow \tilde{A}^2\Pi_u$ excitation spectrum. Balfour[3] reported $\nu_1^+ = 612.6$ cm^{-1} and $2\nu_2^+ = 549.1$ cm^{-1} from the $\tilde{A}^2\Pi_u \rightarrow \tilde{X}^2\Pi_g$ emission spectrum, i.e., his assignment is inverted relative to that of refs 5 and 6. By adopting the interpretation of Balfour, Frey et al.[22] resolved the Fermi polyads of $(\nu_1^+,0,0)^2\Pi_{3/2}$ and $(\nu_1^+ -1,2,0)^2\Pi_{3/2}$ for $\nu_1^+ = 1-3$ and $(\nu_1^+,0,0)^2\Pi_{1/2}$, and $(\nu_1^+ -1,2,0)^2\Pi_{1/2}$ for $\nu_1^+ = 1-2$ in the TPE studies, and reported $\nu_1^+ = 623$ cm^{-1} and $2\nu_2^+ = 559$ cm^{-1}. In our calculations, we obtained $\nu_1^+ = 598.2$ cm^{-1} and $2\nu_2^+ = 518.6$ cm^{-1} (cf. Table 2), in reasonably good agreement with these experiments. As shown below, these theoretical values are also consistent with the assignment of the PFI−PE spectrum, yielding $\nu_1^+ = 613$ cm^{-1} and $2\nu_2^+ = 517$ cm^{-1}. All calculated rovibronic states for J up to 9/2 are given in Table 2. If anharmonic resonances occur, the dominating polyad members for a given J = P state are listed as well.

B. PFI−PE Spectra for $CS_2^+(\tilde{A}^2\Pi_u)$. Figure 3(a) and (b) displays the PFI−PE spectra for $CS_2^+(\tilde{A}^2\Pi_u)$ in the energy regions of 12.61−12.95 eV with a resolution of $\approx$ 4 cm^{-1} (fwhm) and in the energy region of 12.95−13.50 eV with a resolution of $\approx$ 7 cm^{-1} (fwhm), respectively. The peak positions of PFI−PE bands observed in Figure 3(a) and (b) are listed in Table 3. We have also included in Table 3 the peak positions of vibronic bands resolved in the TPE study of Frey et al.,[22] the present theoretical values, and available optical data.[3] The assignment for the majority of PFI−PE bands is achieved by comparison with the theoretical values and optical data. The overall agreement between the calculated rovibronic energies and experimental PFI−PE band positions can be regarded as good, with the largest deviations lying in the range of about 30 cm^{-1}.

Selected high-resolution PFI−PE bands (solid circles, upper spectra) in the regions of 12.685−12.725, 12.760−12.800, 12.830−12.870, and 12.905−12.937 eV are plotted in Figure 4(a), (b), (c), and (d), respectively, for comparison with the corresponding simulated spectra (open circles, lower spectra)

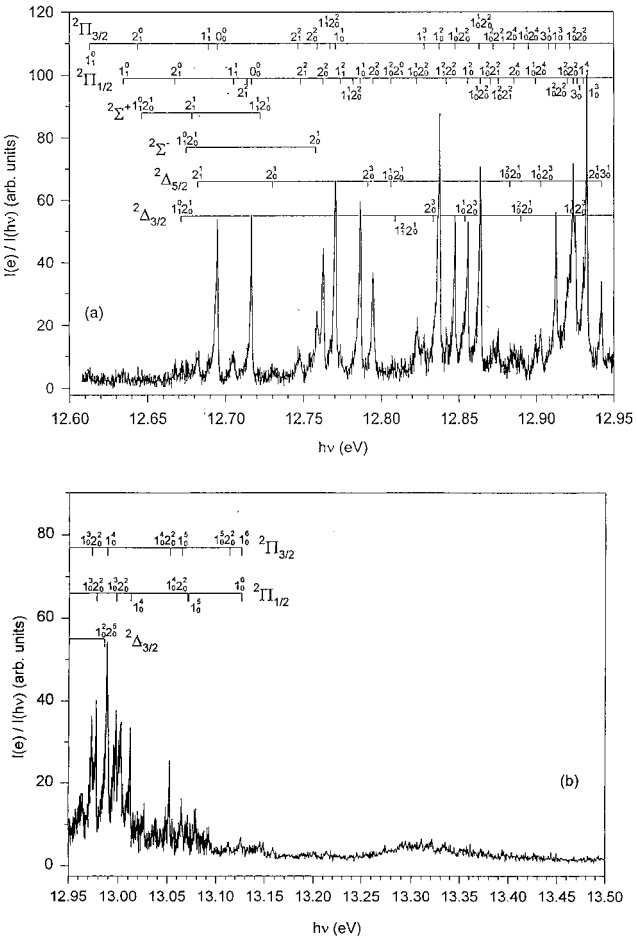

Figure 3. PFI−PE spectrum for the $CS_2^+(A^2\Pi_u)$ state in the region of (a) 12.60−12.95 eV obtained at a PFI−PE resolution of 4 cm^{-1} (fwhm) and (b) 12.95−13.50 eV obtained at a PFI−PE resolution of 7 cm^{-1} (fwhm).

based on the BOS simulation procedures. Experimentally, the individual rotation transitions cannot be resolved. The best fitted BOS coefficients C_λ ($\lambda = 0-4$) and the rotational constants (B^+) for the ionic states used in the simulation are listed in Table 4.

The first two intense peaks with nearly equal intensities in the PFI−PE spectrum of Figure 3(a) can be readily assigned to transitions $(0,0,0)\tilde{A}^2\Pi_{3/2u} \leftarrow (0,0,0)\tilde{X}^1\Sigma_g^+$, and $(0,0,0)\tilde{A}^2\Pi_{1/2u} \leftarrow (0,0,0)\tilde{X}^1\Sigma_g^+$. Both bands are dominated by the $\Delta N = 0$ rotational branch appearing in the middle of the bands. The BOS simulation of these bands shown in Figure 4(a) reproduces the experimental bands quite well using the rotational constant $B'' = 0.1091$ cm^{-1} for neutral state, $B^+ = 0.101$ cm^{-1}, a rotational temperature of 60 K, and a Gaussian line width of 3 cm^{-1}

TABLE 3: Ionization Energies (IEs), Relative Intensities, and Vibrational Assignments for $CS_2^+(\tilde{A}^2\Pi_u)$

IE (eV)[a,b]	G (cm^{-1})[a,b]	theo (cm^{-1})[c]	optical data (cm^{-1})[c,d]	assignment	relative intensity[e]
12.6130	−658	–	(−658.0)	$(0,0,0)^2\Pi_{3/2}-(1,0,0)^1\Sigma_g^+$	6.5
12.6346	−484	(−483.9)	(−480.8)	$(0,0,0)^2\Pi_{1/2}-(1,0,0)^1\Sigma_g^+$	6.2
12.6440	−408	–	(−396.0)	$(0,0,0)^2\Pi_{3/2}-(0,1,0)^1\Pi_u$	7.1
12.6463	−390	(−386.7)	–	$(0,1,0)\mu^2\Sigma^+-(1,0,0)^1\Sigma_g^+$	6.0
12.6676	−218	(−221.9)	(−218.8)	$(0,0,0)^2\Pi_{1/2}-(0,1,0)^1\Pi_u$	9.4
12.6714	−187	(−198.3)	–	$(0,1,0)^2\Delta_{3/2}-(1,0,0)^1\Sigma_g^+$	8.1
12.6746	−161	(−158.0)	–	$(0,1,0)\kappa^2\Sigma^--(1,0,0)^1\Sigma_g^+$	9.1
12.6783	−131	(−124.7)	–	$(0,1,0)\mu^2\Sigma^+-(0,1,0)^1\Pi_u$	7.5
12.6820	−102	(−104.3)	–	$(0,1,0)^2\Delta_{5/2}-(0,1,0)^1\Pi_u$	9.7
12.6889	−46	(−59.8)	(−45.4)	$(1,0,0)^2\Pi_{3/2}-(1,0,0)^1\Sigma_g^+$	10.7
12.6946[f]	0.0	0.0	0.0	$(0,0,0)^2\Pi_{3/2}-(0,0,0)^1\Sigma_g^+$	53.8
(12.6955)	(0.0)				(32)
12.7051	85	(79.0)	(84.0)	$(1,0,0)^2\Pi_{1/2}-(1,0,0)^1\Sigma_g^+$	11.6
12.7137	154	(152.6)	–	$(0,2,0)\mu^2\Pi_{1/2}-(0,1,0)^1\Pi_u$	12.8
12.7166[f]	177.4	174.1	177.2	$(0,0,0)^2\Pi_{1/2}-(0,0,0)^1\Sigma_g^+$	55.0
(12.7189)	(189)				(32)
12.7221	222	(228.5)	–	$(1,1,0)\mu^2\Sigma^+-(1,0,0)^1\Sigma_g^+$	6.7
12.7300	286	291.7	–	$(0,1,0)^2\Delta_{5/2}-(0,0,0)^1\Sigma_g^+$	7.8
12.7464	418	(428.6)	–	$(0,2,0)\kappa^2\Pi_{3/2}-(0,1,0)^1\Pi_u$	13.2
12.7480	431	(429.2)	(412.1)	$(0,2,0)\kappa^2\Pi_{1/2}-(0,1,0)^1\Pi_u^+$	10.9
12.7578	510	500.0	–	$(0,1,0)\kappa^2\Sigma^--(0,0,0)^1\Sigma_g^+$	19.4
12.7587	517	518.6	–	$(0,2,0)\mu^2\Pi_{3/2}-(0,0,0)^1\Sigma_g^+$	24.4
12.7625[f]	548	548.6	549.1	$(0,2,0)\mu^2\Pi_{1/2}-(0,0,0)^1\Sigma_g^+$	44.5
(12.7648)	(559)				(41)
12.7670	584	(549.7)	(574.9)	$(1,2,0)\mu^2\Pi_{3/2}-(1,0,0)^1\Sigma_g^+$	15.5
12.7706[f]	613	598.2	612.6	$(1,0,0)^2\Pi_{3/2}-(0,0,0)^1\Sigma_g^+$	66.1
(12.7727)	(623)				(45)
12.7737	638	(637.0)	(641.4)	$(2,0,0)^2\Pi_{1/2}-(1,0,0)^1\Sigma_g^+$	13.7
12.7818	703	(718.1)	(708.5)	$(1,2,0)\kappa^2\Pi_{1/2}-(1,0,0)^1\Sigma_g^+$	11.5
12.7864[f]	740	737.0	742.0	$(1,0,0)^2\Pi_{1/2}-(0,0,0)^1\Sigma_g^+$	59.5
(12.7898)	(761)				(41)
12.7916	782	782.8	–	$(0,3,0)\mu^2\Delta_{5/2}-(0,0,0)^1\Sigma_g^+$	11.5
12.7947[f]	807	825.2	808.1	$(0,2,0)\kappa^2\Pi_{1/2}-(0,0,0)^1\Sigma_g^+$	36.7
(12.7946)	(799)				(31)
12.8065	903	898.8	–	$(1,1,0)^2\Delta_{5/2}-(0,0,0)^1\Sigma_g^+$	10.2
		(899.0)	(903.4)	$(2,0,0)^2\Pi_{1/2}-(0,1,0)^1\Pi_u$	
12.8090	923	(919.9)	–	$(2,1,0)^2\Delta_{3/2}-(1,0,0)^1\Sigma_g^+$	9.4
12.8230	1036	1026.8	–	$(1,2,0)\mu^2\Pi_{1/2}-(0,0,0)^1\Sigma_g^+$	22.5
12.8278	1074	(1068.4)	(1100.8)	$(3,0,0)^2\Pi_{3/2}-(1,0,0)^1\Sigma_g^+$	17.1
12.8355	1136	1133.8	–	$(0,3,0)\kappa^2\Delta_{3/2}-(0,0,0)^1\Sigma_g^+$	26.8
12.8375[f]	1153	1122.8	1153.2	$(2,0,0)^2\Pi_{3/2}-(0,0,0)^1\Sigma_g^+$	87.7
(12.8401)	(1166)				(57)
12.8420	1189	(1187)	(1190.4)	$(2,2,0)\kappa^2\Pi_{1/2}-(1,0,0)^1\Sigma_g^+$	19.3
12.8476[f]	1234	1207.7	1232.9	$(1,2,0)\mu^2\Pi_{3/2}-(0,0,0)^1\Sigma_g^+$	54.9
(12.8494)	(1241)				(36)
12.8540	1286	1293.7	–	$(1,3,0)\mu^2\Delta_{3/2}-(0,0,0)^1\Sigma_g^+$	24.0
12.8558[f]	1300	1295.0	1299.4	$(2,0,0)\Pi_{1/2}-(0,0,0)^1\Sigma_g^+$	53.0
(12.8574)	(1306)				(43)
12.8632	1360	1367.4	–	$(1,2,0)\kappa^2\Pi_{3/2}-(0,0,0)^1\Sigma_g^+$	53.3
12.8640[f]	1366	1376.1	1366.5	$(1,2,0)\ \kappa^2\Pi_{1/2}-(0,0,0)^1\Sigma_g^+$	70.5
(12.8694)	(1403)				(43)
12.8703	1417	(1415.3)	–	$(2,2,0)\ \mu^2\Pi_{1/2}-(0,1,0)^1\Pi_u$	13.2
12.8722	1432	(1434.6)	(1462.9)	$(2,2,0)\ \mu^2\Pi_{3/2}-(0,1,0)^1\Pi_u$	15.3
12.8757	1461	(1449.0)	(1452.4)	$(2,2,0)\ \kappa^2\Pi_{1/2}-(0,1,0)^1\Pi_u$	18.9
12.8830	1520	1515.1	–	$(2,1,0)^2\Delta_{5/2}-(0,0,0)^1\Sigma_g^+$	14.8
12.8857	1541	1523.6	–	$(0,4,0)\kappa^2\Pi_{1/2}-(0,0,0)^1\Pi_u$	14.2
		1525.0	–	$(0,4,0)\kappa^2\Pi_{3/2}-(0,0,0)^1\Pi_u$	
12.8900	1576	1577.9	–	$(2,1,0)^2\Delta_{3/2}-(0,0,0)^1\Sigma_g^+$	12.8
12.8951	1617	1626.0	–	$(1,4,0)\mu^2\Pi_{3/2}-(0,0,0)^1\Sigma_g^+$	10.0
12.8996	1653	1659.6	–	$(1,4,0)\mu^2\Pi_{1/2}-(0,0,0)^1\Sigma_g^+$	16.8
12.9031	1682	1681.9	–	$(1,3,0)\kappa^2\Delta_{5/2}-(0,0,0)^1\Sigma_g^+$	19.0
12.9082	1723	1709.7	–	$(0,0,1)^2\Pi_{3/2}-(0,0,0)^1\Sigma_g^+$	15.6
12.9127[f]	1759	1726.4	1758.8	$(3,0,0)\ ^2\Pi_{3/2}-(0,0,0)^1\Sigma_g^+$	55.9
(12.9150)	(1770)				(58)
12.9200	1818	1811.3	–	$(2,2,0)\mu^2\Pi_{1/2}-(0,0,0)^1\Sigma_g^+$	35.1
12.9220	1834	1830.6	1858.9	$(2,2,0)\mu^2\Pi_{3/2}-(0,0,0)^1\Sigma_g^+$	41.5
12.9240[f]	1850	1845.0	1848.4	$(2,2,0)\kappa^2\Pi_{1/2}-(0,0,0)^1\Sigma_g^+$	71.4
(12.9258)	(1857)				(100)
12.9255	1862	1861.6	–	$(1,3,0)\kappa^2\Delta_{3/2}-(0,0,0)^1\Sigma_g^+$	51.6
12.9265	1870	1882.8	–	$(0,0,1)^2\Pi_{1/2}-(0,0,0)^1\Sigma_g^+$	24.0
12.9304	1902	–	(1901.5)	$(4,0,0)^2\Pi_{1/2}-(1,0,0)^1\Sigma_g^+$	41.6
12.9327[f]	1920	1906.2	1919.6	$(3,0,0)^2\Pi_{1/2}-(0,0,0)^1\Sigma_g^+$	100
12.9422	1997	2000.5	–	$(0,1,1)^2\Delta_{5/2}-(0,0,0)^1\Sigma_g^+$	33.7

TABLE 3 (Continued)

IE (eV)[a,b]	G (cm^{-1})[a,b]	theo (cm^{-1})[c]	optical data (cm^{-1})[c,d]	assignment	relative intensity[e]
12.9730	2245	2228.8	−	(3,2,0) $\mu^2\Pi_{3/2}-(0,0,0)^1\Sigma_g^+$	36.2
12.9776	2283	2300.3	−	(3,2,0)$\mu^2\Pi_{1/2}-(0,0,0)^1\Sigma_g^+$	40.1
12.9856	2347	2349.4	−	$(2,5,0)^2\Delta_{3/2}-(0,0,0)^1\Sigma_g^+$	27.0
12.9884	2370	−	2366.9	$(4,0,0)^2\Pi_{3/2}-(0,0,0)^1\Sigma_g^+$	54.2
12.9974	2442	2410.1	−	(3,2,0)$\kappa^2\Pi_{1/2}-(0,0,0)^1\Sigma_g^+$	37.7
13.0022	2481	−	−		35.0
13.0119	2559	−	2559.5	$(4,0,0)^2\Pi_{1/2}-(0,0,0)^1\Sigma_g^+$	33.9
13.0522	2884	−	−	(4,2,0)$\mu^2\Pi_{3/2}-(0,0,0)^1\Sigma_g^+$	25.5
13.0646	2984	−	−	$(5,0,0)^2\Pi_{3/2}-(0,0,0)^1\Sigma_g^+$	16.3
13.0700	3028	−	−	(4,2,0)$\kappa^2\Pi_{1/2}-(0,0,0)^1\Sigma_g^+$	10.9
13.0710	3036	−	−	$(5,0,0)^2\Pi_{1/2}-(0,0,0)^1\Sigma_g^+$	12.3
13.0792	3102	−	−		13.9
13.0929	3213	−	−		9.5
13.1133	3377	−	−	$(5,2,0)^2\Pi_{3/2}-(0,0,0)^1\Sigma_g^+$	5.8
13.1255	3475	−	−	$(6,0,0)^2\Pi_{3/2,1/2}-(0,0,0)^1\Sigma_g^+$	6.9

[a] This work. Here IE values are ionization transition energies and ΔE values are energies measured with respect to IE[$A^2\Pi_{3/2}(0_0^0)$]. [b] Parenthetical figures are values from TPE measurement in ref 22. [c] The values in parentheses correspond to hot bands and are obtained by subtracting the known vibrational frequencies of CS_2 from the theoretical predictions or optical data for the ionic states. [d] References 3 and 52. [e] In this work, the intensity for the band $^2\Pi_{1/2}(1_0^3)$ was arbitrarily set to 100, whereas in ref 22, the intensity for the band $\kappa^2\Pi_{1/2}(1_0^2 2_0^2)$ was arbitrarily set to 100. [f] IE values were determined by BOS simulation.

(fwhm). On the basis of BOS fit, we obtain the IE values of 102 389 ± 4 cm^{-1} and 102 566 ± 4 cm^{-1} for the formation of CS_2^+ [$^2\Pi_{3/2u}(0_0^0)$] and CS_2^+ [$^2\Pi_{1/2u}(0_0^0)$], respectively, yielding a spin−orbit splitting constant of −177.4 cm^{-1}. Taking into account the experimental uncertainties, the present IE(CS_2^+ [$^2\Pi_{3/2u}(0_0^0)$]) is in good agreement with that of 102 396 cm^{-1} obtained in the previous TPE study.[22] However, it is apparent that the IE(CS_2^+[$^2\Pi_{3/2u}(0_0^0)$]) value of 102 421 cm^{-1} obtained in the previous HeI study[20] is too high. We note that the recent high-resolution HeI study of Baltzer et al.[21] yielded an IE(CS_2^+[$^2\Pi_{3/2u}(0_0^0)$]) value of 102 378 cm^{-1} and a spin−orbit splitting constant of −175.8 cm^{-1}, which were consistent with the results of the present PFI−PE study.

The direct single-photon ionization transitions to the $\Delta_{5/2}$ and $\Sigma_{1/2}^+$ components of $(0,1,0)CS_2^+(\tilde{X}^2\Pi_g)$ from $(0,0,0)CS_2(\tilde{X}^1\Sigma_g^+)$, although forbidden by the g ⇔ u selection rule, have already been observed in the previous PFI−PE spectra.[12] In the present PFI−PE measurement, the $\Delta_{5/2}(2_0^1)$ is identified at 12.7300 eV and $\kappa^2\Sigma^-(2_0^1)$ at 12.7578 eV based on theoretical predictions. The peaks at 12.6463, 12.6714, 12.6746, 12.6783, and 12.6820 eV are assigned to the hot bands $(0,1,0)\mu^2\Sigma^+ \leftarrow (1,0,0)^1\Sigma_g^+$, $(0,1,0)^2\Delta_{3/2} \leftarrow (1,0,0)^1\Sigma_g^+$, $(0,1,0)\kappa^2\Sigma^- \leftarrow (1,0,0)^1\Sigma_g^+$, $(0,1,0)\mu^2\Sigma^+ \leftarrow (0,1,0)^1\Pi_u$, and $(0,1,0)^2\Delta_{5/2} \leftarrow (0,1,0)^1\Pi_u$, respectively. As indicated in the recent experimental and theoretical study of $OCS^+(\tilde{X}^2\Pi)$,[36] the nonvanishing single-photon ionization cross sections involving the single quantum excitation of the ν_2^+ mode are attributed to the dependence of the electronic part of the integral for the photoionization cross section on the bending coordinate. The electronic transition dipole component changes sign along the positive and negative displacement. Hence, this component in the one-dimensional picture is of ungerade symmetry, as are the one-dimensional cuts of the vibrational bending modes with odd quantum numbers. This could explain why the transition becomes weakly allowed, as observed in OCS^+, CS_2^+, and CO_2^+.[12,36,53,54]

The $^2\Pi_{3/2,1/2u}(1_0^1)$ and $^2\Pi_{3/2,1/2u}(2_0^2)$ bands are located between 12.74 and 12.80 eV. The BOS simulated spectra for these experimental bands [see Figure 4(b)] were obtained using a rotational temperature of 80 K and Gaussian line width of 4 cm^{-1} (fwhm). The other parameters used in the simulation are summarized in Table 4. The IE values determined from simulation are 12.7625, 12.7706, 12.7864, and 12.7947 eV for $\mu^2\Pi_{1/2}(2_0^2)$, $^2\Pi_{3/2}(1_0^1)$, $^2\Pi_{1/2}(1_0^1)$, and $\kappa^2\Pi_{1/2}(2_0^2)$, respectively. The other PFI−PE bands resolved in this region are $\mu^2\Pi_{3/2}(2_0^2)$ at 12.7587 eV, $^2\Delta_{5/2}(2_0^3)$ at 12.7916 eV, and some hot bands originating from $(0,1,0)^1\Pi_u$ and $(1,0,0)^1\Sigma_g^+$ of the neutral CS_2 state. The fact that the energy levels G with respect to $^2\Pi_{3/2}(0_0^0)$ determined here (see Table 3) are in excellent agreement with results obtained by emission studies[3] indicates that the uncertainties for IE values determined in the present PFI−PE measurement are well within the stated uncertainty of 4 cm^{-1}.

The Fermi components associated with $(\nu_1^+, 0, 0)^2\Pi_{3/2u}$ and $(\nu_1^+, 0,0)^2\Pi_{1/2u}$ are $(\nu_1^+-1,2,0)\mu^2\Pi_{3/2}$ and $(\nu_1^+-1,2,0)\kappa^2\Pi_{1/2}$, respectively. The energies and intensities of these states are strongly perturbed by the Fermi resonance interactions. As a result, the spin−orbit splitting (−127 cm^{-1}) for $^2\Pi_{3/2,1/2u}(1_0^1)$ is found to be significantly lower than that for $^2\Pi_{3/2,1/2u}(0_0^0)$. The observation of lower intensity for the $^2\Pi_{1/2u}(1_0^1)$ band as compared to that for the $^2\Pi_{3/2u}(1_0^1)$ band can also be attributed to the intensity trade between the Fermi resonance interaction of $^2\Pi_{1/2u}(1_0^1)$ and $\kappa^2\Pi_{1/2}(2_0^2)$.

On the basis of the BOS simulation [Figure 4(c)], we obtained IE values of 12.8375, 12.8476, 12.8558 and 12.8640 eV for the PFI−PE bands $^2\Pi_{3/2}(1_0^2)$, $\mu^2\Pi_{3/2}(1_0^1 2_0^2)$, $^2\Pi_{1/2}(1_0^2)$ and $\kappa^2\Pi_{1/2}(1_0^1 2_0^2)$, respectively. The BOS simulation shown in Figure 4(d) gives IE values 12.9127, 12.9240, and 12.9327 eV for the respective PFI−PE bands $^2\Pi_{3/2}(1_0^3)$, $\kappa^2\Pi_{1/2}(1_0^2 2_0^2)$, and $^2\Pi_{1/2}(1_0^3)$. We note that the G values for energy levels determined based on these IE values are in excellent agreement with those obtained in the emission studies. The TPE results[22] seem to be too high by about 10 cm^{-1}.

We assign the respective peaks at 12.9082 and 12.9265 eV as $^2\Pi_{3/2u}(3_0^1)$ and $^2\Pi_{1/2u}(3_0^1)$, and the peak at 12.9422 eV as $^2\Delta_{5/2}(2_0^1 3_0^1)$. This yields a value of 1723 cm^{-1} for ν_3^+. In $CO_2^+(\tilde{A}^2\Pi_u)$, the asymmetric stretch frequency is much larger than those in the $CO_2^+(\tilde{X}^2\Pi_g$ and $\tilde{B}^2\Sigma_u^+)$ states.[53−55] One can therefore also expect an increase in ν_3^+ of $CS_2^+(\tilde{A}^2\Pi_u)$ relative to that of $CS_2^+(\tilde{X}^2\Pi_g)$. The ν_3^+ mode has not been assigned in previous HeI and TPE studies. The only reported value of $2\nu_3^+ = 3288$ cm^{-1} was from the excitation spectrum of Bondybey et al.[6] However, their assignment is different from ours.

In the high-energy side of the PFI−PE spectrum (12.97−13.13 eV), several Fermi polyads involving high excitation of both the stretching and bending modes are resolved. For example, one can see the $^2\Pi_{3/2,1/2}(1_0^4)$ and $^2\Pi_{3/2,1/2}(1_0^3 2_0^2)$ levels at 12.97−13.01 eV, the $^2\Pi_{3/2,1/2}(1_0^5)$ and $^2\Pi_{3/2,1/2}(1_0^4 2_0^2)$ levels

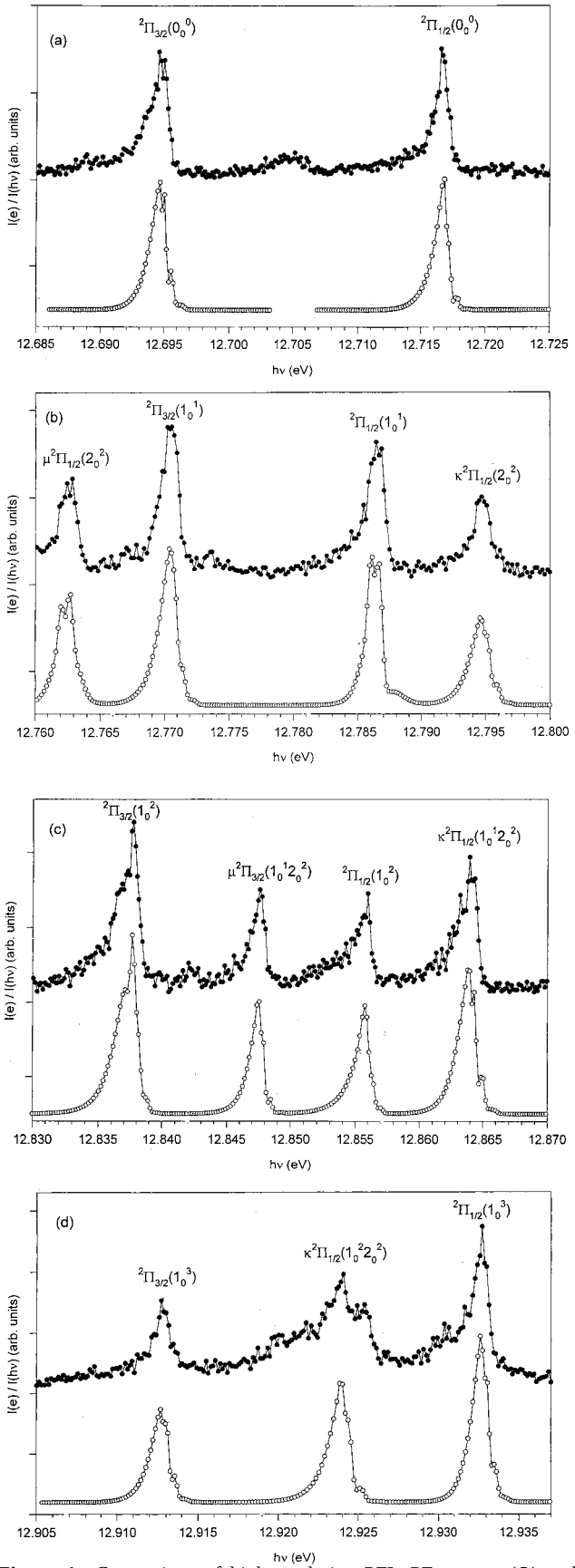

Figure 4. Comparison of high-resolution PFI−PE spectra (●) and simulated spectra (○) for CS_2^+. (a) $^2\Pi_{3/2}(0_0^0)$ and $^2\Pi_{1/2}(0_0^0)$ bands in the energy range of 12.685−12.725 eV; (b) $^2\Pi_{3/2,1/2}(1_0^1)$ and $^2\Pi_{3/2,1/2}(2_0^2)$ bands in the energy range of 12.76−12.80 eV; (c) $^2\Pi_{3/2,1/2}(1_0^2)$ and $^2\Pi_{3/2,1/2}(1_0^12_0^2)$ bands in the energy range of 12.83−12.87 eV; and (d) $^2\Pi_{3/2,1/2}(1_0^3)$ and $^2\Pi_{1/2}(1_0^22_0^2)$ bands in the energy range of 12.905−12.937 eV. PFI−PE resolution = 4 cm^{-1} (fwhm).

TABLE 4: The Rotational Constants (B^+) and BOS Coefficients (C_λ, $\lambda = 0-4$) Used in the Simulation of the PFI−PE Bands for CS_2^+

state	B^+ (cm^{-1})[a]	C_0	C_1	C_2	C_3	C_4
$^2\Pi_{3/2}(0_0^0)$	0.101	0	0.769	0	0	0.231
$^2\Pi_{1/2}(0_0^0)$	0.101	0	0.901	0	0.090	0.009
$\mu^2\Pi_{1/2}(2_0^2)$	0.109	0	0.714	0	0	0.286
$^2\Pi_{3/2}(1_0^1)$	0.109	0	0.833	0	0	0.167
$^2\Pi_{1/2}(1_0^1)$	0.101	0	0.909	0	0	0.091
$\kappa^2\Pi_{1/2}(2_0^2)$	0.102	0	0.588	0	0	0.412
$^2\Pi_{3/2}(1_0^2)$	0.098	0	0.909	0	0	0.091
$\mu^2\Pi_{3/2}(1_0^12_0^2)$	0.097	0	0.800	0	0.100	0.100
$^2\Pi_{1/2}(1_0^2)$	0.101	0	0.825	0.083	0.082	0.010
$\kappa^2\Pi_{1/2}(1_0^12_0^2)$	0.101	0	0.653	0	0	0.347
$^2\Pi_{3/2}(1_0^3)$	0.100	0	0.625	0.083	0.083	0.209
$\kappa^2\Pi_{1/2}(1_0^22_0^2)$	0.100	0	0.750	0	0	0.250
$^2\Pi_{1/2}(1_0^3)$	0.103	0	0.800	0	0.200	0

[a] The differences in B^+ values are within the experimental uncertainty and thus are not physically significant.

at 13.05−13.10 eV, and the $^2\Pi_{3/2,1/2}(1_0^6)$ and $^2\Pi_{3/2}(1_0^52_0^2)$ levels at 13.10−13.13 eV. All of these peaks are listed in Table 3. We note that for such highly excited levels, the attribution into ν_1^+ and ν_2^+ quantum numbers is somewhat artificial due to anharmonic and Fermi resonances and polyads interactions.

In the energy region above 13.13 eV, the intensity of PFI−PE bands decreases. The calculations indicate that most of the PFI−PE bands in the higher energy region are strongly mixed so that the assignment of the vibrational quantum numbers is not possible. As stressed by Frey et al.,[22] strong autoionization peaks may occur above the $(3,0,0)^2\Pi_u$ state, which may further complicate the structure of the spectrum in this region.

The recent photoelectron study of Baltzer et al. using HeI, HeII, and synchrotron radiation represents the most comprehensive photoelectron study of the valence photoelectron bands of CS_2.[21] Although the resolution of 5 meV (fwhm) achieved in the latter experiment is poorer than that of the present PFI−PE study, the main photoelectron features observed in the HeI spectrum for $CS_2^+(A^2\Pi_u)$ are generally consistent with those resolved in the present PFI−PE spectrum. There are some differences in the relative intensities of vibronic bands observed in the PFI−PE and HeI photoelectron spectra. For example, in the PFI−PE spectrum the peak around 12.9327 eV is the most intense, whereas in the HeI spectrum the most intense peak is at 12.8364 eV. It is well known that the intensities for PFI−PE bands depend on perturbation of near resonance autoionizing Rydberg states and the lifetime effect of high-n ($n \geq 100$) Rydberg states involved.[35−41] Because the mechanism for the population of vibronic bands in HeI photoionization is different from that in PFI−PE studies, the different vibronic band intensities observed in these studies are not surprising.

IV. Conclusions

We performed a high-resolution PFI−PE study of CS_2 in the region of 12.61−13.50 eV using the high-resolution VUV synchrotron facility at the Chemical Dynamics Beamline of the ALS. This article covers the formation of PFI−PE bands for $CS_2^+(\tilde{A}^2\Pi_u; \nu_1^+ = 0-6, \nu_2^+ = 0-4, \nu_3^+ = 0-1)$ states. With the aid of theoretical Renner−Teller calculations, we satisfactorily assigned vibronic bands resolved in the PFI−PE spectrum for $CS_2^+(\tilde{A}^2\Pi_u)$. The Fermi polyads up to $\nu_1^+ = 6$ were identified. The excitation of the ν_3^+ mode was also found in the complex rovibronic progression. The BOS simulation of the high-resolution PFI−PE bands for $CS_2^+(\tilde{A}^2\Pi_u; \nu_1^+ = 0-3, \nu_2^+ = 0, 2, \nu_3^+ = 0)$ provided accurate IE values for these states.

Acknowledgment. The authors thank Dr. C.-W. Hsu, Dr. M. Evans, and Dr. S. Stimson for their help in obtaining PFI-PE data for this system. This work was supported by the Director, Office of Energy Research, Office of Basic Energy Sciences, Chemical Sciences Division of the U.S. Department of Energy under Contract No. DE-AC03-76SF00098 for the Lawrence Berkeley National Laboratory and Contract No. W-7405-Eng-82 for the Ames Laboratory. C.Y.N. acknowledges partial support by AFOSR. M.H. acknowledges the NERSC (University of California at Berkeley), the CCR (University of Paris VI), and the computational center of the University of Marne-la-Vallée for computational time. This work has been supported by the EC-contract HPRN-CT-1999-00005.

References and Notes

(1) Hudson, R. D. *Rev. Geophys. Space Phys.* **1970**, *9*, 305.
(2) Lee, L. C.; Judge, D. L.; Ogawa, M. *Can. J. Phys.* **1975**, *53*, 1861.
(3) Balfour, W. J. *Can. J. Phys.* **1976**, *54*, 1969.
(4) Endoh, M.; Tsuji, M.; Nishimura, Y. *Chem. Phys. Lett.* **1984**, *109*, 35.
(5) Bondybey, V. E.; English, J. H.; Miller, T. A. *J. Chem. Phys.* **1979**, *70*, 1621.
(6) Bondybey, V. E.; English, J. H. *J. Chem. Phys.* **1980**, *73*, 3098.
(7) Tanaka, Y.; Jursa, A. S.; LeBlanc, F. J. *J. Chem. Phys.* **1960**, *32*, 1205.
(8) Ogawa, M.; Chang, H. C. *Can. J. Phys.* **1970**, *48*, 2455.
(9) Trott, W. M.; Blais, N. C.; Walters, E. A. *J. Chem. Phys.* **1979**, *71*, 1692.
(10) Ono, Y.; Linn, S. H.; Prest, H. F.; Gress, M. E.; Ng, C. Y. *J. Chem. Phys.* **1980**, *73*, 2523.
(11) Fisher, I.; Lochschmidt, A.; Strobel, A.; Niedner-Schatteburg, G.; Müller-Dethlefs, K.; Bondybey, V. E. *Chem. Phys. Lett.* **1993**, *202*, 542.
(12) Huang, J.-C.; Cheung, Y.-S.; Evans, M., Liao, C.-X.; Ng, C. Y.; Hsu, C.-W.; Heimann, P.; Lefebvre-Brion, H.; Cossart-Magos, C. *J. Chem. Phys.* **1997**, *106*, 864.
(13) Eland, J. H. D.; Danby, C. J. *Int. J. Mass. Spectrom. Ion Phys.* **1968**, *1*, 111.
(14) Collin, J. E.; Natalis, P. *Int. J. Mass Spectrom. Ion Phys.* **1968**, *1*, 121.
(15) Brundle, C. R.; Turner, D. W. *Int. J. Mass. Spectrom. Ion Phys.* **1969**, *2*, 195.
(16) Potts, A. W.; Fattahallah, G. H. *J. Phys. B: At. Mol. Phys.* **1980**, *13*, 2545.
(17) Hubin-Franskin, M.-J.; Delwiche, J.; Natalis, P.; Caprace, G. *J. Electron Spectrosc. Relat. Phenom.* **1980**, *18*, 295.
(18) Kovaè, B. *J. Chem. Phys.* **1983**, *78*, 1684.
(19) Reineck, I.; Wannberg, B.; Veehuizen, H.; Nohre, C.; Maripuu, R.; Norell, K.-E.; Mattsson, L.; Karlsson, L.; Siegbahn, K. *J. Electron Spectrosc. Relat. Phenom.* **1984**, *34*, 235.
(20) Wang, L. S.; Reutt, J. E.; Lee, Y. T.; Shirley, D. A. *J. Electron Spectrosc. Relat. Phenom.* **1988**, *47*, 167.
(21) Baltzer, P.; Wannberg, B.; Lundqvist, M.; Karlsson, L.; Holland, D. M. P.; MacDonald, M. A.; Hayes, M. A.; Tomasello, P.; von Niessen, W. *Chem. Phys.* **1996**, *202*, 185.
(22) Frey, R.; Gotchev, B.; Peatman, W. B.; Pollak, H.; Schlag, E. W. *Int. J. Mass Spectrom. Ion Phys.* **1978**, *26*, 137.
(23) Maier, J. P.; Thommen, F. *Chem. Phys.* **1980**, *51*, 319.
(24) Schirmer, J.; Domcke, W.; Cederbaum, L. S.; Von Niessen, W., Åsbrink, L. *Chem. Phys. Lett.* **1979**, *61*, 30.
(25) Nakatsuji, H. *Chem. Phys.* **1983**, *76*, 283.
(26) Chin, S.; Person, W. B. *J. Phys. Chem.* **1984**, *88*, 553.
(27) Brommer, M.; Rosmus, P. *Chem. Phys. Lett.* **1993**, *206*, 540.
(28) Suits, A. G.; Heimann, P.; Yang, X.; Evans, M.; Hsu, C−W.; Blank, D. A.; Lu, K−T.; Kung, A.; Lee, Y. T. *Rev. Sci. Instrum.* **1995**, *66*, 4841.
(29) Hsu, C−W.; Evans, M.; Heimann, P.; Lu, K−T.; Ng, C. Y. *J. Chem. Phys.* **1996**, *105*, 3950.
(30) Heimann, P.; Koike, M.; Hsu, C.−W.; Evans, M.; Lu, K. T.; Ng, C. Y.; Suits, A.; Lee, Y. T. *Rev. Sci. Instrum.* **1997**, *68*, 1945.
(31) Hsu, C.-W.; Evans, M.; Ng, C. Y.; Heimann, P. *Rev. Sci. Instrum.* **1997**, *68*, 1694.
(32) Hsu, C.-W.; Heimann, P. A.; Evans, M.; Stimson, S.; Fenn, T.; Ng, C. Y. *J. Chem. Phys.* **1997**, *106*, 8931.
(33) Evans, M.; Ng, C. Y.; Hsu, C.-W.; Heimann, P. *J. Chem. Phys.* **1997**, *106*, 978.
(34) Shiell, R. C.; Evans, M.; Stimson, S.; Hsu, C.-W.; Ng, C. Y.; Hepburn, J. W. *Phys. Rev. Lett.* **1998**, *80*, 472.
(35) Stimson, S.; Chen, Y.-J.; Evans, M.; Liao, C.-L.; Ng, C. Y.; Hsu, C.-W.; Heimann, P. *Chem. Phys. Lett.* **1998**, *289*, 507.
(36) Stimson, S.; Evans, M.; Ng, C. Y.; Destandau, C.; Chambaud, G.; Rosmus, P.; Hsu, C.-W.; Heimann, P. *J. Chem. Phys.* **1998**, *108*, 6205.
(37) Hsu, C.-W.; Evans, M.; Stimson, S.; Ng, C. Y. *J. Chem. Phys.* **1998**, *108*, 4701.
(38) Hsu, C.-W.; Evans, M.; Stimson, S.; Ng, C. Y. *J. Chem. Phys.* **1998**, *109*, 1285.
(39) Evans, M.; Stimson, S.; Ng, C. Y.; Hsu, C.-W.; Jarvis, G. K. *J. Chem. Phys.* **1999**, *110*, 315.
(40) Song, Y.; Evans, M.; Ng, C. Y.; Hsu, C.-W.; Jarvis, G. K. *J. Chem. Phys.* **1999**, *111*, 1905.
(41) Jarvis, G. K.; Evans, M.; Ng, C. Y.; Mitsuke, K. *J. Chem. Phys.* **1999**, *111*, 3058.
(42) Cairns, R. B.; Samson, J. A. R. *J. Opt. Soc. Am.* **1966**, *56*, 1568.
(43) Hsu, C.-W.; Evans, M.; Stimson, S.; Ng, C. Y.; Heimann, P. *Chem. Phys.* **1998**, *231*, 121.
(44) (a) Knowles, P. J.; Werner, H.-J. *Chem. Phys. Lett.* **1985**, *115*, 259. (b) Roos, P.; Taylor, P.; Siegbahn, E. M. *Chem. Phys.* **1980**, *48*, 157.
(45) Werner, H.-J.; Knowles, P. J. *J. Chem. Phys.* **1988**, *89*, 5803.
(46) Knowles, P. J.; Knowles, H.-J. *Chem. Phys. Lett.* **1988**, *145*, 514.
(47) Dunning, T. H. *J. Chem. Phys.* **1989**, *90*, 1007.
(48) MOLPRO is a package of ab initio programs written by Werner, H. J.; Knowles, P. J., with contributions from Amos, R. D.; Berning, A.; Cooper, D. L.; Deegan, M. J. O.; Dobbyn, A. J.; Eckert, F.; Hampel, C.; Leininger, T.; Lindh, R.; Loyd, A. W.; Meyer, W.; Mura, M. E.; Niclass, A.; Palmieri, P.; Peterson, K.; Pitzer, R.; Pulay, P.; Rauhut, G.; Schuetz, M.; Stoll, H.; Stone, A. J.; Thorsteinsson, T. Further details can be obtained at www.tc.bham.ac.uk/molpro.
(49) Carter, S.; Handy, N. C. *Mol. Phys.* **1984**, *52*, 1367.
(50) Carter, S.; Handy, N. C.; Rosmus, P.; Chambaud, G. *Mol. Phys.* **1990**, *71*, 605.
(51) Buckingham, A. D.; Orr, B. J.; Sichel, J. M. *Philos. Trans. R. Soc. London, Ser. A*, **1970**, *268*, 147.
(52) Herzberg, G. *Molecular Spectra and Molecular Structure III, Electronic Spectra and Electronic Structure of Polyatomic Molecules*; Krieger: Malabar, FL, 1991.
(53) Liu, J.; Chen, W.; Hsu, C.-W.; Hochlaf, M.; Evans, M.; Stimson, S.; Ng, C. Y. *J. Chem. Phys.* **2000**, *112*, 10767.
(54) Baltzer, P.; Chau, F. T.; Eland, J. H. D.; Karlsson, L.; Lundqvist, M.; Rostas, J.; Tam, K. Y.; Veenhuizen, H.; Wannberg, B. *J. Chem. Phys.* **1996**, *104*, 8922.
(55) Liu, J.; Hochlaf, M.; Ng, C. Y. *J. Chem. Phys.*, in press.